Failure Mechanism of Rock Specimens with a Notched Hole Under Compression - A Numerical Study

Amin Manouchehrian
JiangXi University of Science and Technology
Pinnaduwa H.S.W. Kulatilake
JiangXi University of Science and Technology
Rui Wu (wurui@jxust.edu.cn)
JiangXi University of Science and Technology https://orcid.org/0000-0001-5082-0267

Case study

Keywords: Rock, Fracturing, Notch, Compression, Numerical modeling

Posted Date: May 13th, 2021

DOI: https://doi.org/10.21203/rs.3.rs-515335/v1

Failure mechanism of rock specimens with a notched hole under compression - A numerical study

Amin Manouchehrian, Pinnaduwa H.S.W. Kulatilake, Rui Wu*

School of Resources and Environmental Engineering, Jiangxi University of Science and Technology, Ganzhou 341000, China

Abstract

Discontinuities are natural structures that exist in rocks and can affect the stability of rock structures. In this article, the influence of notch presence on the failure evolution around a hole in compressed rock specimens is investigated numerically. Firstly, the uniaxial compressive test on a rock specimen with a circular hole is modeled and the failure evolution in the specimen is simulated. In a separate model, notches are created at the surface of the hole. Results show that when the notches are created in the model, failure zone around the hole is transferred to a distance away from the surface of the hole. In addition, a parametric study is carried out to investigate the influence of the notch length and the confining pressure on the fracturing behavior of the specimen. Numerical results presented in this article indicate that the presence of notches at the surface of the hole and their dimensions can affect the fracturing mechanism of the specimen. In some cases, the failure at the boundary of the hole is prevented when the notches of certain dimensions are added to the hole. The insights gained from this numerical study may be helpful to control the failure around underground excavations.

Keywords: Rock; Fracturing; Notch; Compression; Numerical modeling.

1. Introduction

Discontinuity is an inherent characteristic of rocks and rock-like materials. Generally, rocks include defects and discontinuities at various scales. Different types of defect exist in rocks

such as faults, bedding planes, pores, grain boundaries, joints, holes, cracks, and notches. These natural defects originate from the various geological processes acting on the rocks. Moreover, defects in rock may be created artificially for some engineering purposes. Whether the defects are formed naturally or created artificially, they affect the load-bearing capacity of the rock (Brace 1961; Cai et al. 2004; Howarth and Rowlands 1987; Kemeny 2005). Defects in rock masses are stress raisers and play a key role in the rock fracturing processes. Therefore, understanding the role of different types of defect on the mechanical behavior of rocks under various loading conditions is an essential task for any rock engineering design.

Cracks and notches are two types of planar defects that may exist naturally in rock masses or may be created artificially in different structures such as dams, tunnels, and wells. The definition of a "crack" refers to a defect that is generated during the loading process and a "notch" or a "flaw" refers to a prefabricated defect in the solids. Cracks and notches show a similar behavior under tensile loads, however, their behavior under compressive and shear stresses are different. When a crack is subjected to pure compression, the two faces of the crack are pushed together and the free space between them closes due to the penetration of the molecules on each face into the other face. In this condition, the presence of the crack has a little or no effect on the strength of the solid. Thus, the crack behavior under pure compression (negative Mode-I) is not crucial to the stability of a structure. In contrast, a notch under compression can affect the stability of a solid depending on the distance between the two faces of the notch and its geometry,

In rock structures, rocks are subjected to different loading conditions. Damage initiation and propagation from a pre-existing defect in rock depends on the loading condition. In theory, three basic modes of crack extension are postulated: opening mode (Mode-I), shearing mode (Mode-II), and tearing mode (Mode-III). Basic modes of crack extension are sketched in Figure 1. In the rock mechanics and the fracture mechanics literature, a large number of studies have been devoted to the study of initiation, propagation and coalescence of cracks in rocks and brittle materials under different loading conditions (Gehle and Kutter 2003;

Kulatilake et al. 2001; Le et al. 2018; Lee and Jeon 2011; Lee and Ravichandran 2003; Manouchehrian et al. 2014; Park and Bobet 2010; Wang et al. 2011; Wong and Einstein 2009; Wong and Chau 1998; Wu et al. 2019c; Yang et al. 2013; Zhang et al. 2009; Zhuang et al. 2014). These studies revealed many fracturing characteristics of rocks and led to the improvement of safety in rock structures.

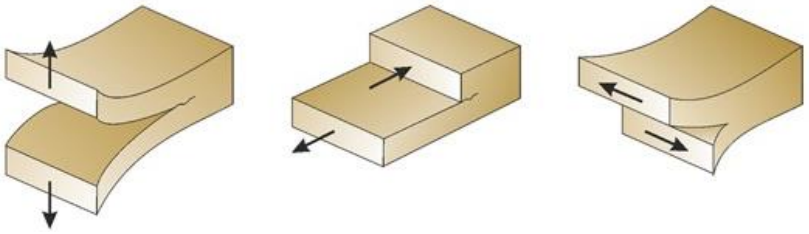

Figure 1. Basic modes of crack extension

In the studies related to failure mechanism of defected rock specimens (including cracks, flaws, notches, etc.), tensile and shear loads are usually more applied while the pure compression is neglected. In rock structures such as mine pillars, tunnel walls, and slopes, the existing defects at the surface of the excavations are subjected mainly to pure compression. Hence, the influence of presence of a defect on the failure evolution of rocks under compression is important. The fracturing behavior of defects under pure compression has been studied in a limited number of investigations (Berto et al. 2013; Bura et al. 2019; Torabi et al. 2015). For example, Berto et al. (2013) used polycrystalline graphite to study the brittle failure of specimens with V-shaped notches under pure compression. They observed and explained the failure evolution from the notch tips. In a similar experiment, Bura et al. (2019) studied the fracturing process in polymethyl methacrylate (PMMA) specimens under compression which were weakened by V and U-shaped edge notches. In their research, fracture evolution during the notch closure was observed. Torabi et al. (2015) suggested a flattened V-notched semi-disk specimen to study brittle failure of PMMA specimens with

blunt V-shaped notches under compression. These studies showed that the failure behavior of notches under compression has some specific characteristics.

In this research, a numerical study is conducted to understand how the failure mechanism of specimens with a circular hole would change if notches exist at the surface of the hole. In Section 2, the stress distribution around circular holes and cracks under Mode-I loading condition is described. In Section 3, bonded particle models are built to study the failure mechanism of a specimen with a notched hole under compression. In Section 4, a parametric study is conducted to investigate the influence of the notch length and the confining pressure on the failure behavior of the specimen.

2. Stress state around circular holes and cracks under Mode-I loading condition

Prior to any excavation, rock mass is subjected to lithostatic stress field. Upon excavation, the stresses around the excavation are redistributed to reach an equilibrium state. The stress state after excavation depends on the geometry of the opening in addition to the rock material properties, and boundary and loading conditions. Generally, the geometry of openings is designed in a way to minimize the stress concentration at the boundaries of the excavation to prevent the consequent instabilities. Among the basic geometrical shapes, a hole with a circular cross-section has the minimum stress concentration factor at its boundary in a homogeneous, continuous and isotropic medium (Sharma 2011). In the classical mechanics, the stress state around a circular hole in an infinite plate can be calculated using the closed form solution. Figure 2 shows an infinite plate with a hole subjected to a two-directional stress field in which $\sigma_x = K\sigma_\infty$ and $\sigma_y = \sigma_\infty$. The stress state around a circular hole under two-directional stress field in an infinite plate is (Hubbert and Willis 1972)

$$\sigma_r = \frac{\sigma_\infty}{2}\left[(1+K)\left(1-\frac{a^2}{r^2}\right) - (1-K)\left(1-4\frac{a^2}{r^2}+3\frac{a^4}{r^4}\right)cos2\theta\right] \qquad (1)$$

$$\sigma_\theta = \frac{\sigma_\infty}{2}\left[(1+K)\left(1+\frac{a^2}{r^2}\right)+(1-K)\left(1+3\frac{a^4}{r^4}\right)cos2\theta\right] \quad (2)$$

$$\tau_{r\theta} = \frac{\sigma_\infty}{2}\left[(1-K)\left(1+2\frac{a^2}{r^2}-3\frac{a^4}{r^4}\right)sin2\theta\right] \quad (3)$$

where σ_r, σ_θ and $\tau_{r\theta}$ are radial, tangential and shear stresses, respectively. It should be noted that the stress state around an opening is not dependent on the mechanical properties of the material. By placing $r = a$ in Eqs.1 through 3, the stress state at a circular hole boundary in an infinite plate is

$$\sigma_r = 0 \quad (4)$$

$$\sigma_\theta = \sigma_\infty[(1+K)+2(1-K)cos2\theta] \quad (5)$$

$$\tau_{r\theta} = 0 \quad (6)$$

According to Eq.5, in a stress field in which K<1, the maximum principal stress is concentrated at the side walls ($\theta = 0, \pi$) and the minimum principal stress is located at the top ($\theta = \frac{\pi}{2}$) and bottom ($\theta = \frac{3\pi}{2}$) of the hole boundary.

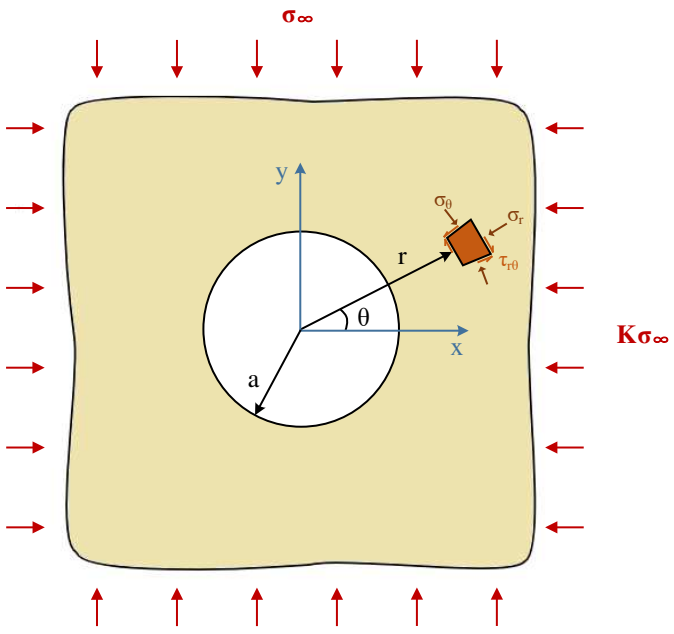

Figure 2. The used coordinate system to express the stress state around a circular hole in a two directional stress field

The fracture mechanics provides solutions for calculation of the stress and displacement in the solids in which cracks exist. Generally, the fracture mechanics provides accurate solutions for brittle elastic materials. For a given crack, its extension may be accomplished in one or more modes (Figure 1). The near crack tip (r<<l) stresses under opening mode loads (Mode-I) can be calculated using Irwin's concept of the stress intensity factors, which characterize the strength of the singularity at a crack tip (Figure 3) (Anderson 2017), as follows:

$$\sigma_{xx} = \frac{\sigma_\infty \sqrt{\pi b}}{\sqrt{2\pi r}} cos\frac{\theta}{2}\left[1 - sin\frac{\theta}{2} sin\frac{3\theta}{2}\right] \quad (7)$$

$$\sigma_{yy} = \frac{\sigma_\infty \sqrt{\pi b}}{\sqrt{2\pi r}} cos\frac{\theta}{2}\left[1 + sin\frac{\theta}{2} sin\frac{3\theta}{2}\right] \quad (8)$$

$$\tau_{xy} = \frac{\sigma_\infty \sqrt{\pi b}}{\sqrt{2\pi r}} sin\frac{\theta}{2} cos\frac{\theta}{2} cos\frac{3\theta}{2} \quad (9)$$

where b is the half-length of the crack. Eqs.7 through 9 suggest that the maximum stress concentration happens at the tips of the crack.

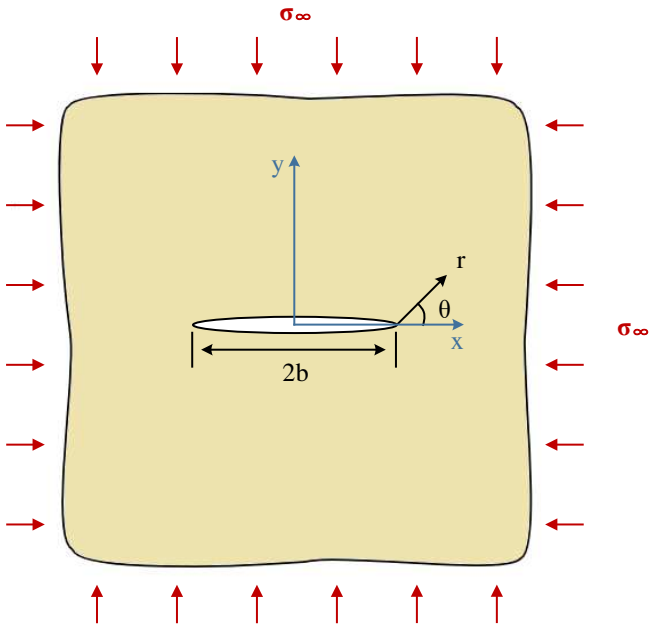

Figure 3. The used coordinate system to express the stress state near a crack tip in a two directional stress field

Usually, the analytical methods give solutions with a good accuracy for calculation of the stress state around the openings for simple geometry. For example, the stress state in a plate with a hole (Figure 4a) or a crack (Figure 4b) subjected to compression can be easily calculated. However, there is no analytical solution to calculate the stress state if these two

basic geometries are combined (Figure 4c). In the real-world, the engineering problems contain components with complex geometries which make it difficult to use analytical solutions for engineering designs.

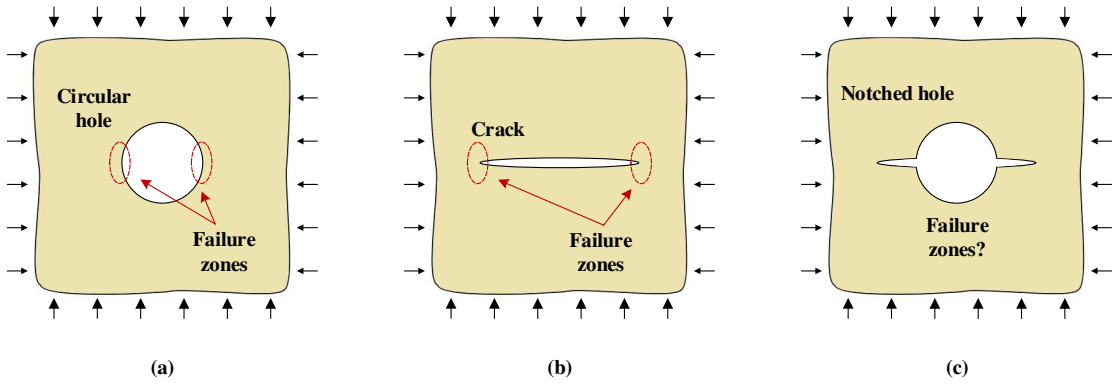

Figure 4. Failure zones in specimens with (a) a circular hole, (b) a crack, and (c) a notched hole under compression

Advanced computational models empower scientists and engineers to build more complex and more detailed models for solving problems. Presence of notches at the surface of a hole (Figure 4c) and its influence on the stress distribution around the hole can be simulated using advanced computational models. In a recent study, the authors used FEM models to study the stress distribution around a notched circular tunnel under compression. They showed that when notches are created in the tunnel, the adjacent rock at the sides of the notches is destressed and the stress concentration zones are transferred to a distance away from the wall (Figure 5). In that study, they concluded that the presence of notches at a tunnel wall might be capable of changing the failure pattern at the wall in a favorable manner (Manouchehrian and Kulatilake 2021). In the present study, bonded particle models are used to simulate the fracturing process around a notched hole.

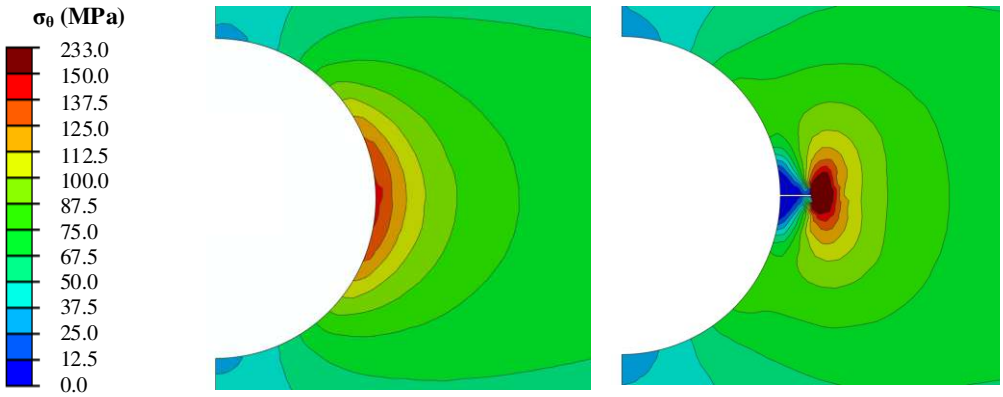

Figure 5. The tangential stress distribution around (a) a regular tunnel and (b) a notched tunnel

3. Simulation of failure in a rock specimen with a notched hole

The available analytical solutions in the classical mechanics and the fracture mechanics are usually applicable for solving simple problems. To simulate complex engineering problems, advanced numerical models are needed. Successful application of different numerical methods such as the finite element method (FEM), extended finite element method (XFEM), discrete/distinct element method (DEM), boundary element method (BEM), and displacement discontinuity method (DDM) have proved merits of numerical models for simulation of fracture evolution in solids (Fatehi Marji and Dehghani 2010; Javanmardi and Maheri 2019; Manouchehrian and Marji 2012; Peng et al. 2017; Schöpfer et al. 2009; Sukumar et al. 2000; Tan et al. 1998; Wu et al. 2019a; Wu et al. 2019b). In this section, simulation of failure evolution in rock specimens with a notched hole is discussed.

3.1.Model setup

In this study, the bonded particle models are developed to simulate the fracturing process in rock specimens. In the bonded particle models, the cracking process is simply simulated by breakage of bonds between particles. This is a simple approach for simulation of cracking in comparison to some other methods in which the crack evolution is simulated by solving complex mathematical equations related to fracture mechanics. For implementation of the

bonded particle models, Particle Flow Code (PFC) (Itasca 2004) is utilized. Because the purpose of this study is to simulate the fracturing behavior of rectangular prismatic specimens, the problem can be simplified to a plane strain problem. Therefore, in this study the two-dimensional version of the code (PFC^{2D}) is used.

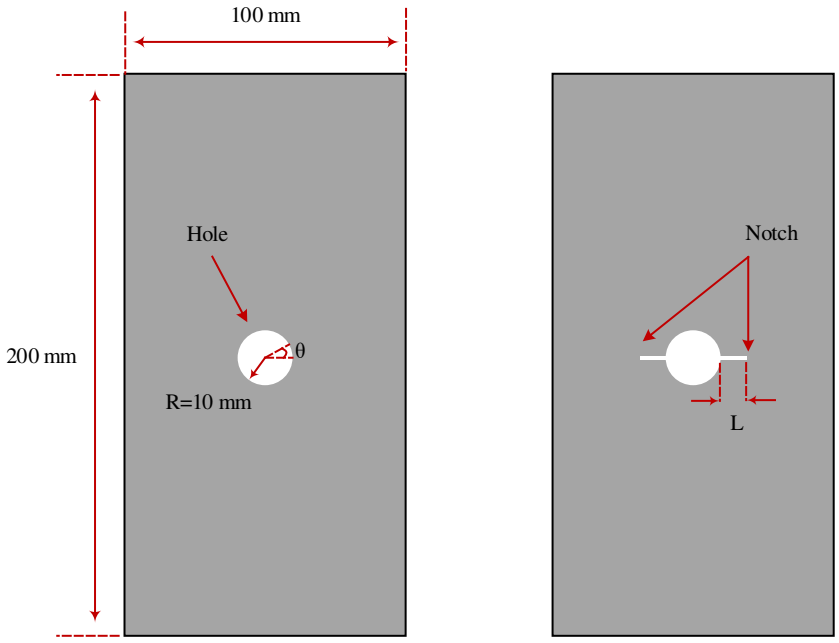

(a) Circular hole (b) Notched hole

Figure 6. Geometry of the models with (a) a circular hole and (b) a notched hole

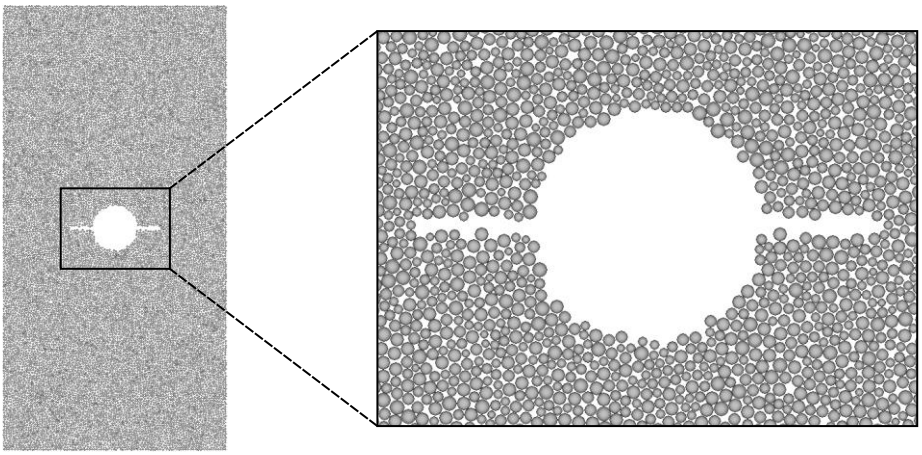

Figure 7. Particle assembly in the notched hole model (L = 10 mm)

In PFC modeling, it is not straightforward to assign the physical and mechanical properties of materials. The models need to be calibrated by changing several micro-parameter values to

obtain macro-parameter values for such as the elastic and the plastic properties of the material. For this purpose, usually the unconfined and confined compressive tests as well as the Brazilian test are simulated. In the calibration process, different micro-parameter values are varied to calibrate the model to get the desired macro-parameter values of the material. The procedures given by Yang et al. (2015) and Mehranpour and Kulatilake (2017) were used as guidance to perform the calibration process. The calibrated micro-parameter values and the used macro-parameter values for the simulated rock specimens in this study are listed in Table 1 and Table 2, respectively. The macro-parameter values of the simulated rock represent typical mechanical properties of soft rocks such as shale and marl and rock-like materials such as concrete.

Table 1. PFC^{2D} calibrated micro-mechanical parameters for the simulated rock specimen

Micro-parameters	Value
Particle minimum radius, R (mm)	0.4
Particle radius ratio, R_{max}/R_{min}	1.66
Particle density (kg/m^3)	2000
Particle contact modulus, E_c (GPa)	6.1
Particle stiffness ratio, k_n/k_s	1.0
Particle friction coefficient, μ	0.5
Parallel-bond modulus, $\bar{E}_c$ (GPa)	6.1
Parallel-bond stiffness ratio, $\bar{k}_n/\bar{k}_s$	1.0
Parallel-bond radius multiplier, $\bar{\lambda}$	1.0
Parallel-bond normal strength, mean (MPa)	12
Parallel-bond normal strength, std. dev. (MPa)	2.0
Parallel-bond shear strength, mean (MPa)	12
Parallel-bond shear strength, std. dev. (MPa)	2.0

Table 2. The macro-mechanical parameters for the simulated rock specimen

Macro-parameters	Value
Uniaxial compressive strength, σ_c (MPa)	18.95
Tensile strength, σ_t (MPa)	2.92
Young Modulus, E (GPa)	10.02
Poisson ratio, υ	0.11
Cohesion, c (MPa)	7.03
Internal friction angle, φ (°)	18

In this study a rectangular rock specimen with a width of 100 mm and a height of 200 mm is simulated including the mechanical properties listed in Table 2. The geometry of the models

is shown in Figure 6. The simulated specimen includes a rectangular assembly of 18892 circular particles. The radius of the particles follows a Gaussian distribution function with the minimum and the maximum radii of 0.4 mm and 0.66 mm, respectively. After reproduction of the rectangular assembly, the circular hole and notches are created by removing the particles at the appropriate locations. The circular hole with a radius of R = 10 mm is created at the center of the specimen (See Figure 6). The notches are created by removing the particles in a narrow strip with a width of 1.5 mm. This approach is appropriate for simulation of open cracks. Simulation of closed and filled cracks can be done by assigning zero tensile strength to the bonds of neighbor particles in a straight line or by using smooth joint models (Mehranpour and Kulatilake 2017). The particle assembly of a notched hole with the length of L = 10 mm is illustrated in Figure 7. The pushing forces to the specimen's ends are applied by moving two parallel rigid walls toward each other in the direction of the loading. In this paper, the models containing a central circular hole is referenced as "the circular hole" (Figure 6a) and the models which include notches at the surface of the hole is referenced as "the notched hole" (Figure 6b). It should be noted that in this study, one particle assembly is used in all models. In this way, only the influences of the geometry and the boundary condition changes are considered.

3.2.Failure evolution in the circular hole and the notched hole

In this section, models with and without notches are built to study the effect of notches on the failure behavior of rock specimens under compression. Firstly, the uniaxial compression test on a rectangular specimen with a circular hole is simulated (Figure 6a). The stress-strain curve for this specimen is plotted in Figure 8. In this figure, the stress-strain curve obtained from the uniaxial compressive test on the intact rock specimen (i.e. with no hole and no notches) is also plotted. The figure shows that the specimen with a central circular hole reaches a maximum stress of 15.65 MPa before it fails. This is 17.4% less than that in the intact specimen in which the maximum uniaxial strength is 18.95 MPa.

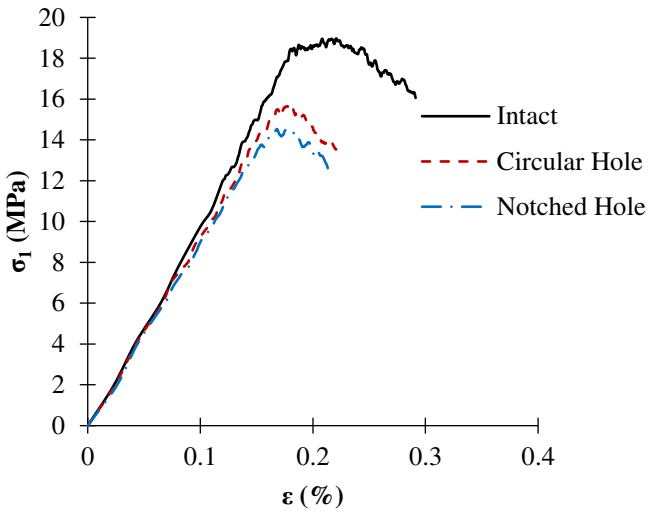

Figure 8. The stress-strain curves obtained from PFC^{2d} models

Figure 9a shows the failure evolution in the specimen with the circular hole. In this figure, the failure patterns at the 75% peak stress, 90% peak stress, peak stress and 80% post-peak stress are illustrated. The black and the yellow lines in Figure 9 represent the tensile and the shear cracks, respectively. When the specimen is loaded at 75% peak stress, a few cracks are nucleated at the left side of the hole (θ = 180°) where the tangential stress is concentrated (see Eq. 5). In addition, tensile cracks are formed at the bottom of the hole (θ = 270°). Also, some minor cracks appear in the specimen which are mainly distributed around the hole. At 90% of the peak stress level, more fractures are formed around the hole and localized failure zones appear at the two sides of the hole (θ = 0° and 180°). At the peak stress, the cracks are coalesced and formed into obvious failure planes. Figure 10a shows a close view of the failure zone at the left side of the hole at the peak stress level. In this figure, the rock at the surface of the hole is crushed because it is the location of the maximum tangential stress around the circular hole (Eq. 5). By applying more strain to the model and bringing it to the 80% of the peak stress (post-peak), the number of cracks is increased, and the failure planes become wider.

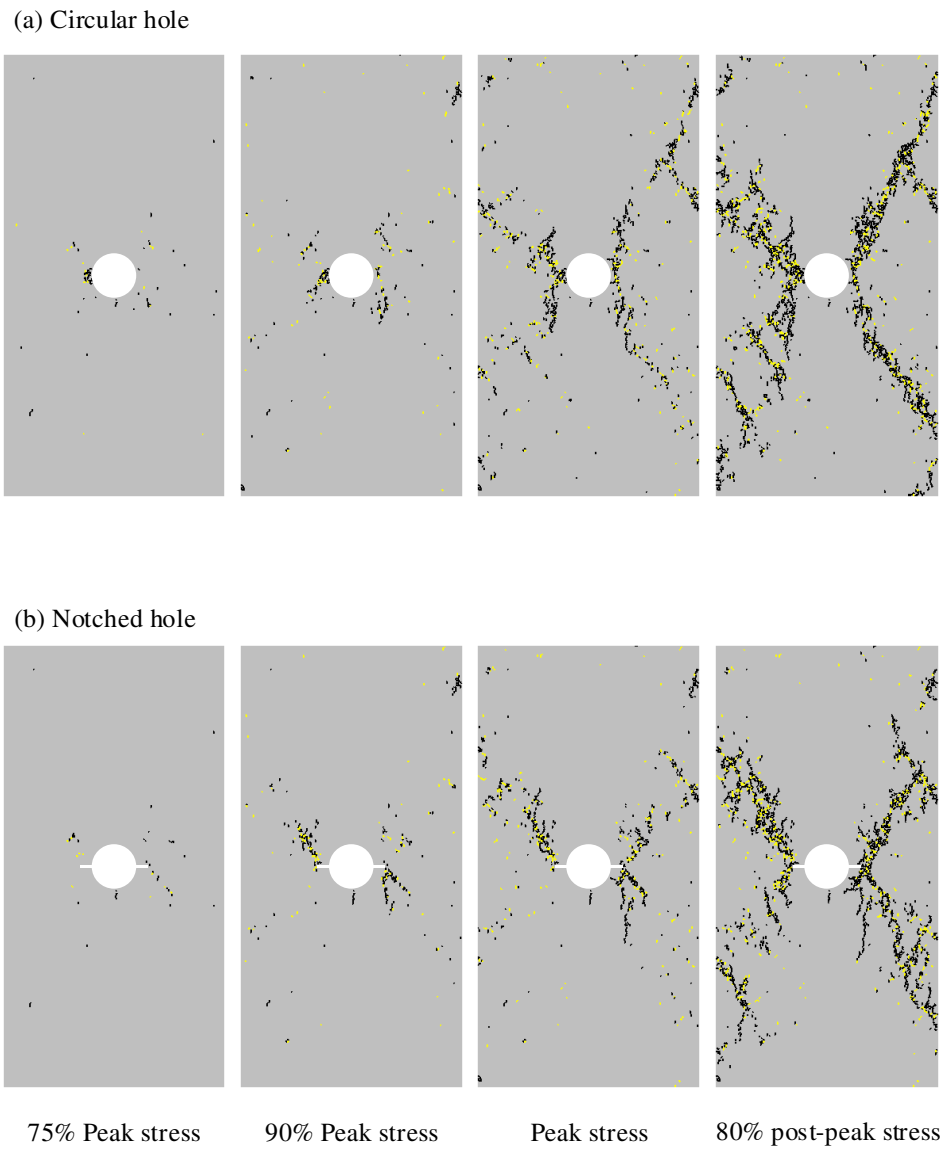

Figure 9. Failure evolution in (a) circular hole, and (b) notched hole (Black and yellow lines represent tensile and shear cracks, respectively)

In a separate model, two notches with the length of L = 5 mm, which results in L/R = 0.5, are created on the wall of the hole at θ = 0° and 180° (see Figure 6b). This model is referenced as the notched hole. The same modeling procedure explained in Section 3.1 is used. The stress-strain curve for this model is shown in Figure 8. The figure shows a maximum strength of 14.53 MPa for the notched hole model. This is 7.1% and 23.3% less than that in the circular hole model and the intact model, respectively.

The failure evolution in the notched hole model is shown in Figure 9b. The figure indicates that first a minor tensile crack is formed at the bottom of the hole (θ = 270°). In the notched

model, the free space at the wall created by notches allows more vertical displacement to the particles around the notches. Consequently, more tensile stress is induced at the top and bottom of the hole. Thus, the formed tensile cracks at the bottom of the model are longer than that in the circular hole model. Moreover, some minor cracks are formed in the specimen which are mainly localized around the hole. The free space created by the hole and the notches allow the particles to slide toward the free space. At 90% peak stress, some cracks are nucleated from tips of the notches where the stress concentration zones exist (Eqs.7 to 9). These cracks are coalesced and create two major fracture planes. At the peak stress, the cracks are propagated and form clear failure planes. At 80% post-peak stress, the failure planes become wider and are extended to the boundaries of the specimen.

A close view of the failure zones around the notched hole at the peak stress level is shown in Figure 10b. The figure indicates that the failure in the notched hole model is mainly developed from the tip of the notch while the rock at the two sides of the notch is not fractured. In the circular hole, a load bearing closed ring has occurred in the rock around the hole (Figure 11a). When a notch is created, the free space provided by the notch destroys this closed ring of rock (Figure 11b) and destress the adjacent rock (see Figure 5b). It explains the integrity of the rock that exists at the sides of the notch in Figure 10b. However, at high stresses the notch may get closed and the rocks at the notch sides may get reloaded (Manouchehrian and Kulatilake 2021).

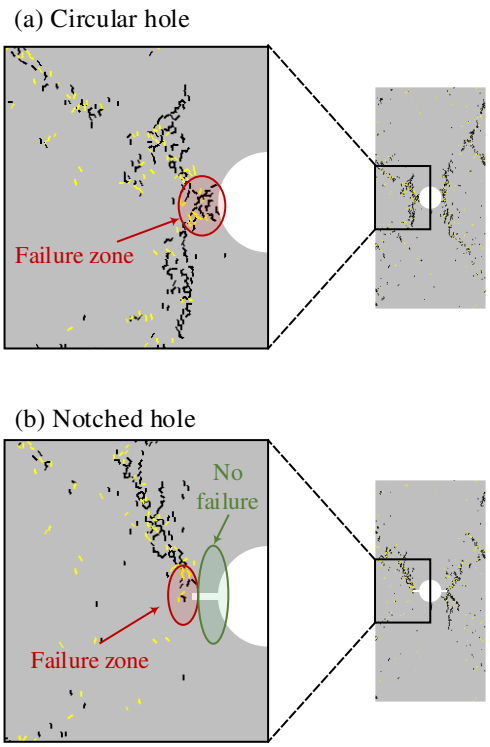

Figure 10. The close views of failure zones around at left side of the hole at peak-stress in the models with (a) a circular hole, and (b) a notched hole with L = 5 mm

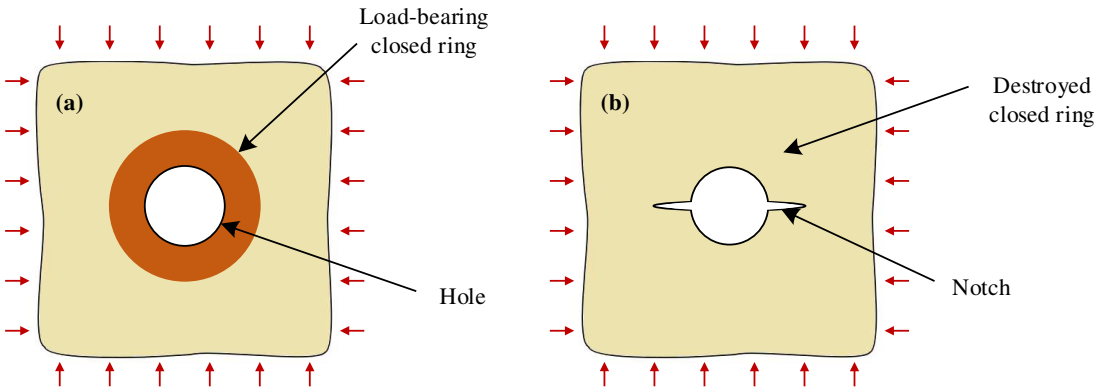

Figure 11. Illustration of the load bearing closed ring around a circular hole

3.3.Influence of the notch length on the failure mechanism

A rectangular specimen including a hole with a radius of R = 10 mm is modeled. Two notches are created on the wall of the hole at θ = 0° and 180° in the model. The length of the notch is varied using L = 2.5, 5, 7.5, and 10 mm, resulting in L/R ratios of 0.25, 0.5, 0.75, and 1, respectively. The model size, material properties and boundary conditions explained in Section 3.1 are used.

The failure patterns in the models with different notch lengths at 80% post-peak stress level are illustrated in Figure 12. The figure shows that when the length of the notch is increased, the tensile failure at the bottom of the hole is longer. In the models with longer notches, the free space resulted from the notches is larger; therefore, a higher number of particles can move towards the free space. As a result, more tensile stress is induced at the top (θ = 90°) and bottom of the hole (θ = 270°). Figure 12 indicates that in the models with different notch lengths, cracks are mainly formed at the tips of the notches. In the models with longer notches, the failure zone is far away from the hole wall. When the length of the notch is decreased, the failure zone is closer to the wall of the hole. The failure pattern around the notched hole in the model with L = 2.5 mm (L/R ratio of 0.25) is shown in Figure 13a. The figure indicates that in this model, the formed cracks are turned back toward the hole surface and resulted in the failure of the rock at the wall (θ = 0° and 180°). The displacement vectors of the particles in this model are shown in Figure 13b. The figure indicates higher displacements of the particles at this location (θ = 315° to 0°) compared to the other particles in the model domain. It means that at the right wall of the hole, the particles moved toward the hole. This can be interpreted as possible rock failure and fall in the hole in the real-world situation for circular holes with short notch lengths. The failure patterns given in Figure 13 indicate that it is possible to select L/R ratios including a minimum value, which depends on the in-situ stresses, rock material properties as well as the boundary and loading conditions, to prevent failure occurring at the wall of the hole. From the numerical results presented in this section, it can be concluded that the influence of the notches on the fracturing mechanism around a hole is a function of the notch dimensions.

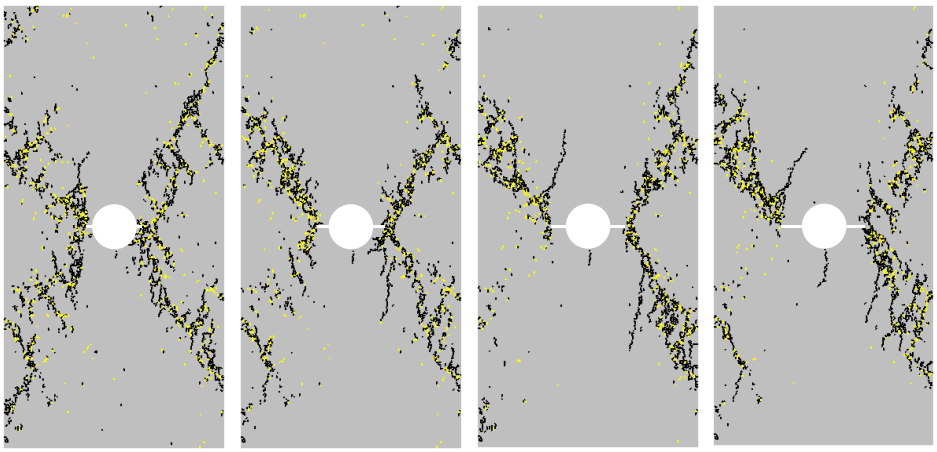

L = 2.5 mm L = 5 mm L = 7.5 mm L = 10 mm

Figure 12. The failure patterns in the models with different notch lengths (80% post-peak stress)

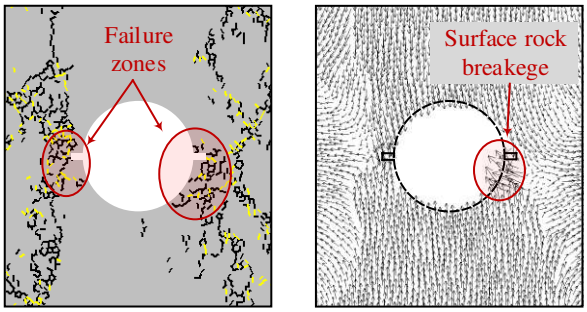

(a) Failure pattern (b) displacement vectors

Figure 13. Failure pattern and displacement vector distribution around the notched hole with L = 2.5 mm (*L/R* ratio of 0.25)

3.4. Influence of confinement on the failure mechanism

In an underground rock structure, the rock mass is usually subjected to confined loading conditions. Therefore, evaluation of rock behavior under confinement is an essential task for any rock engineering design. In this section, some models are built to study the failure behavior of rock specimens with a notched hole under different confining pressures. This type of loading condition can represent the stress state around an underground circular tunnel. Two notches with the length of L = 5 mm (L/R ratio of 0.50) at the wall of the hole are included in the model. The confining pressure is varied with σ_3 = 0, 2, 4, and 6 MPa. The model size, material properties and boundary conditions explained in Section **Error! Reference source not found.**3.1 are used.

Firstly, the influence of the confinement on the failure mechanism in the specimens with a circular hole (Figure 6a) is investigated. The failure pattern in the specimens subjected to different confining pressures is shown in Figure 14a. The figure shows the failure patterns at 80% post-peak stress level. In Figure 14a, when the confinement is zero the fractures are accumulated at the wall of the hole (θ = 0°, 180°). For this case, a minor tensile fracture is formed at the bottom of the hole. The failure planes are extended to the external boundaries of the models which represent the rupture of the specimen. With the increase in the confinement, larger volumes of rock around the hole are fractured. Also, the width of the shear bands becomes wider. The influence of the confinement on the peak strength of the specimens is shown in Figure 15. This figure indicates that the strength of the specimen with a circular hole increases with the increase of the confinement.

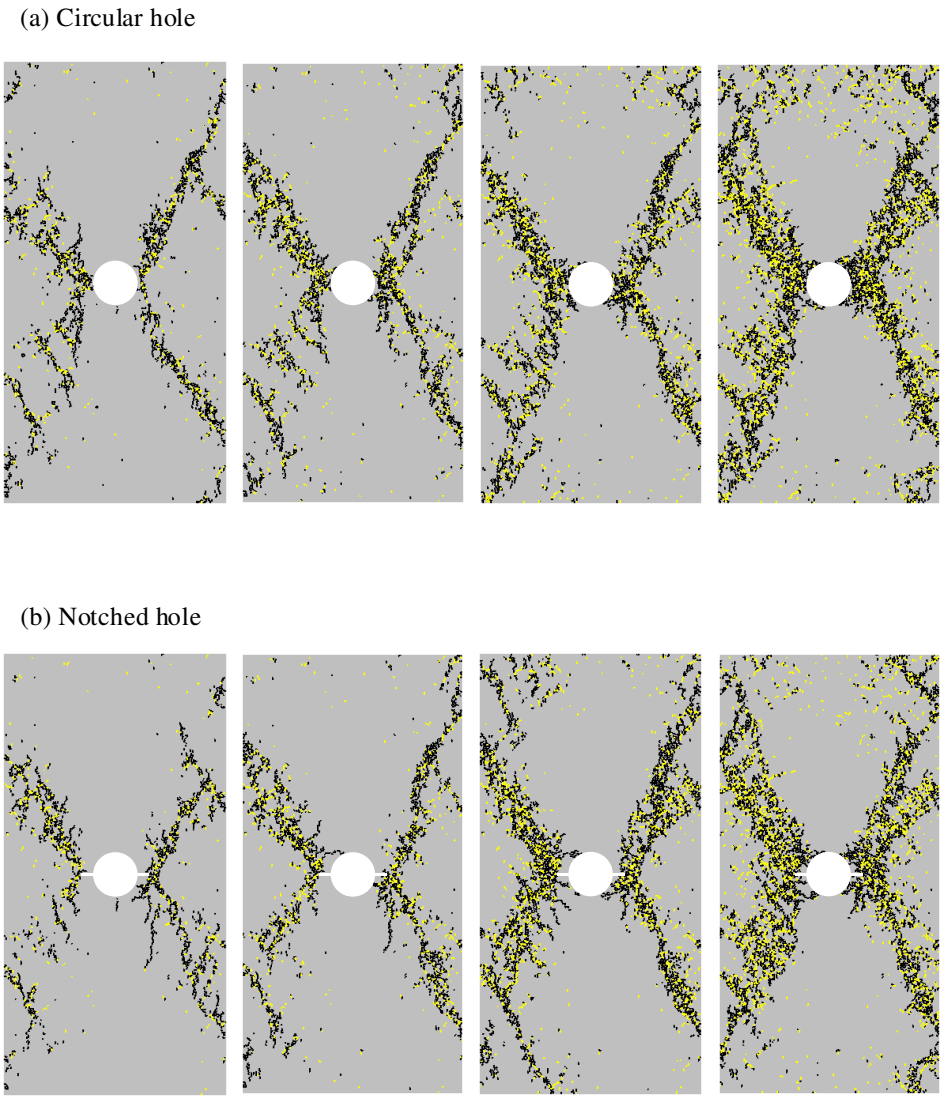

Figure 14. Failure patterns in the (a) circular hole and (b) notched hole models at 80% post-peak stress level for different confining pressures

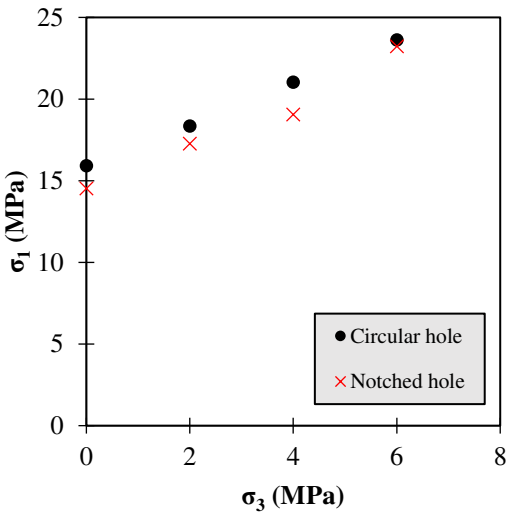

Figure 15. The peak strength at different confining pressures in the two models

Next, the influence of the confinement on the failure mechanism in the specimens with a notched hole (Figure 6b) is studied. Two notches with the length of L = 5 mm (L/R ratio of 0.50) are created in the model. In Figure 14b, when the confinement is zero, the failures are nucleated from the notch tips. Some minor tensile fractures are formed at the bottom of the hole (θ = 270°), where the tensile stress is maximum. At higher confinements, this tensile cracking does not appear. When the confining pressure is increased to 2 MPa, a few cracks turned back toward the surface of the hole (θ = 135° and 315°). However, a larger portion of the volume of the rock at the sides of the notches is remained unfractured. In the models with higher confinements, the damage to the rock at the wall of the hole has increased. Figure 14b shows that when the confinement is 6 MPa, cracks coalesced and created crushed zones around the hole. Figure 15 indicates that the strength of the specimen in the notched hole models are slightly smaller than that in the circular hole model. However, at 6 MPa the difference between the two afore-mentioned strengths becomes negligible. Figure 14b and Figure 15 show that in the simulated notched hole (L =5 mm; L/R ratio of 0.50), the notches affect the failure mechanism at confinements up to 4 MPa. Under higher confining pressures, the notches do not play any meaningful role in fracturing mechanism.

4. Conclusions

Discontinuity is an intrinsic characteristic of rocks which may exist in rocks in different shapes and sizes. The failure behavior of defects such as cracks and notches in rocks and brittle materials under different loading conditions has been studied in the previous rock mechanics and fracture mechanics studies. However, the failure behavior of defects under pure compression (negative Mode-I) is neglected in the previous studies. In this research, a numerical study was conducted to understand how the failure mechanism of specimens containing a circular hole would change if notches exist at the surface of the hole. Firstly, the uniaxial compressive test on a rock specimen with a circular hole was modeled and the failure evolution in the specimen was simulated. In a separate model, two notches were created at the surface of the hole. Results showed that when the notches were created in the model, failure zones around the hole were transferred to the tips of the notches and the rock at the sides of the notches remained unfractured.

Next, a parametric study was carried out to investigate the influence of the notch length on the fracturing behavior of the specimen. It was found that the influence of the notches on the fracturing mechanism around a hole is a function of the notch dimensions. Moreover, the influence of the confinement on the failure mechanism in the specimens with a circular hole was investigated. Results showed that the notches affect the failure mechanism at confinements up to 4 MPa. Under higher confining pressures, the notches do not play any meaningful role in fracturing mechanism.

The numerical modeling results presented in this study showed that the presence of defects (notches in this study) at the surface of a hole can affect the fracturing mechanism of the rock around that hole. In some cases, the failure at the boundary of the hole was prevented when the notches above a certain *L/R* ratio were created in the model. It implies that the notches might be useful to control the failures at the underground excavation boundaries. It is important to point out that the minimum *L/R* ratio to prevent failure at the boundary of the hole depends on the in-situ stresses, material properties as well as the boundary and loading

conditions. Therefore, numerical modeling should be performed incorporating the site-specific data to obtain the minimum *L/R* ratio. In addition, the validity of the numerical results should be examined in practice through physical modeling. In future, we plan to conduct some laboratory experiments to verify the reliability of the numerical results.

Acknowledgements

The financial supports the first author received from the Jiangxi University of Science and Technology (Fund No. 205200100469), the second author received from the Distinguished Foreign Expert Talent Program Funding and the third author received from the National Natural Science Foundation of China (Fund No. 51604126) are gratefully acknowledged.

Conflicts of interest/Competing interests: The authors declare that they have no known competing financial interests or personal relationships that could have appeared to influence the work reported in this paper.

Availability of data and material: The data appearing in the manuscript can be made available by contacting the first author of the manuscript after publishing the paper.

Code availability: Authors have no ownership of the computer code used in this paper. It should be purchased from Itasca Consulting Company.

References

Anderson TL (2017) Fracture mechanics: fundamentals and applications. CRC press,

Berto F, Lazzarin P, Ayatollahi MR (2013) Brittle fracture of sharp and blunt V-notches in isostatic graphite under pure compression loading Carbon 63:101-116 doi:https://doi.org/10.1016/j.carbon.2013.06.045

Brace WF (1961) Dependence of Fracture Strength of Rocks on Grain Size. Paper presented at the The 4th U.S. Symposium on Rock Mechanics (USRMS), University Park, Pennsylvania, 1961/1/1/

Bura E, Derpeński Ł, Seweryn A (2019) Fracture in PMMA notched specimens under compression – Experimental study Polymer Testing 77:105923 doi:https://doi.org/10.1016/j.polymertesting.2019.105923

Cai M, Kaiser PK, Uno H, Tasaka Y, Minami M (2004) Estimation of rock mass deformation modulus and strength of jointed hard rock masses using the GSI system International Journal of Rock Mechanics and Mining Sciences 41:3-19 doi:https://doi.org/10.1016/S1365-1609(03)00025-X

Fatehi Marji M, Dehghani I (2010) Kinked crack analysis by a hybridized boundary element/boundary collocation method International journal of solids and structures 47:922-933 doi:https://doi.org/10.1016/j.ijsolstr.2009.12.008

Gehle C, Kutter HK (2003) Breakage and shear behaviour of intermittent rock joints International Journal of Rock Mechanics and Mining Sciences 40:687-700 doi:https://doi.org/10.1016/S1365-1609(03)00060-1

Howarth DF, Rowlands JC (1987) Quantitative assessment of rock texture and correlation with drillability and strength properties Rock Mech Rock Engng 20:57-85 doi:10.1007/bf01019511

Hubbert MK, Willis DG (1972) Mechanics of hydraulic fracturing

Itasca (2004) PFC 3D Manual, Version 3.1 Itasca Consulting Group, Minneapolis

Javanmardi MR, Maheri MR (2019) Extended finite element method and anisotropic damage plasticity for modelling crack propagation in concrete Finite Elements in Analysis and Design 165:1-20 doi:https://doi.org/10.1016/j.finel.2019.07.004

Kemeny J (2005) Time-dependent drift degradation due to the progressive failure of rock bridges along discontinuities International Journal of Rock Mechanics and Mining Sciences 42:35-46 doi:https://doi.org/10.1016/j.ijrmms.2004.07.001

Kulatilake PHSW, Malama B, Wang J (2001) Physical and particle flow modeling of jointed rock block behavior under uniaxial loading International Journal of Rock Mechanics and Mining Sciences 38:641-657 doi:https://doi.org/10.1016/S1365-1609(01)00025-9

Le H, Sun S, Kulatilake Pinnaduwa HSW, Wei J (2018) Effect of Grout on Mechanical Properties and Cracking Behavior of Rock-Like Specimens Containing a Single Flaw under Uniaxial Compression International Journal of Geomechanics 18:04018129 doi:10.1061/(asce)gm.1943-5622.0001225

Lee H, Jeon S (2011) An experimental and numerical study of fracture coalescence in pre-cracked specimens under uniaxial compression International journal of solids and structures 48:979-999 doi:https://doi.org/10.1016/j.ijsolstr.2010.12.001

Lee S, Ravichandran G (2003) Crack initiation in brittle solids under multiaxial compression Engineering Fracture Mechanics 70:1645-1658 doi:https://doi.org/10.1016/S0013-7944(02)00203-5

Manouchehrian A, Kulatilake PHSW (2021) Feasibility study of a conceptualized destressing method for strainburst control Manuscript submitted for publication

Manouchehrian A, Marji MF (2012) Numerical analysis of confinement effect on crack propagation mechanism from a flaw in a pre-cracked rock under compression Acta Mechanica Sinica 28:1389-1397

Manouchehrian A, Sharifzadeh M, Marji MF, Gholamnejad J (2014) A bonded particle model for analysis of the flaw orientation effect on crack propagation mechanism in brittle materials under compression Archives of civil and mechanical engineering 14:40-52

Mehranpour MH, Kulatilake PHSW (2017) Improvements for the smooth joint contact model of the particle flow code and its applications Computers and Geotechnics 87:163-177 doi:https://doi.org/10.1016/j.compgeo.2017.02.012

Park CH, Bobet A (2010) Crack initiation, propagation and coalescence from frictional flaws in uniaxial compression Engineering Fracture Mechanics 77:2727-2748 doi:https://doi.org/10.1016/j.engfracmech.2010.06.027

Peng X, Atroshchenko E, Kerfriden P, Bordas SPA (2017) Isogeometric boundary element methods for three dimensional static fracture and fatigue crack growth Computer Methods in Applied Mechanics and Engineering 316:151-185 doi:https://doi.org/10.1016/j.cma.2016.05.038

Schöpfer MPJ, Abe S, Childs C, Walsh JJ (2009) The impact of porosity and crack density on the elasticity, strength and friction of cohesive granular materials: Insights from DEM modelling International Journal of Rock Mechanics and Mining Sciences 46:250-261 doi:https://doi.org/10.1016/j.ijrmms.2008.03.009

Sharma DS (2011) Stress concentration around circular/elliptical/triangular cutouts in infinite composite plate. Paper presented at the Proceedings of the world congress on engineering 2011, London,

Sukumar N, Moës N, Moran B, Belytschko T (2000) Extended finite element method for three-dimensional crack modelling International Journal for Numerical Methods in Engineering 48:1549-1570 doi:https://doi.org/10.1002/1097-0207(20000820)48:11<1549::AID-NME955>3.0.CO;2-A

Tan XC, Kou SQ, Lindqvist PA (1998) Application of the DDM and fracture mechanics model on the simulation of rock breakage by mechanical tools Engineering Geology 49:277-284 doi:https://doi.org/10.1016/S0013-7952(97)00059-8

Torabi AR, Firoozabadi M, Ayatollahi MR (2015) Brittle fracture analysis of blunt V-notches under compression International journal of solids and structures 67-68:219-230 doi:https://doi.org/10.1016/j.ijsolstr.2015.04.022

Wang QZ, Feng F, Ni M, Gou XP (2011) Measurement of mode I and mode II rock dynamic fracture toughness with cracked straight through flattened Brazilian disc impacted by split Hopkinson pressure bar Engineering Fracture Mechanics 78:2455-2469 doi:https://doi.org/10.1016/j.engfracmech.2011.06.004

Wong LNY, Einstein HH (2009) Systematic evaluation of cracking behavior in specimens containing single flaws under uniaxial compression International Journal of Rock Mechanics and Mining Sciences 46:239-249 doi:https://doi.org/10.1016/j.ijrmms.2008.03.006

Wong RHC, Chau KT (1998) Crack coalescence in a rock-like material containing two cracks International Journal of Rock Mechanics and Mining Sciences 35:147-164 doi:https://doi.org/10.1016/S0148-9062(97)00303-3

Wu H, Kulatilake PHSW, Zhao G, Liang W (2019a) Stress distribution and fracture evolution around a trapezoidal cavity in sandstone loaded in compression Theoretical and Applied Fracture Mechanics 104:102348 doi:https://doi.org/10.1016/j.tafmec.2019.102348

Wu H, Kulatilake PHSW, Zhao G, Liang W, Wang E (2019b) A comprehensive study of fracture evolution of brittle rock containing an inverted U-shaped cavity under uniaxial compression Computers and Geotechnics 116:103219 doi:https://doi.org/10.1016/j.compgeo.2019.103219

Wu H, Zhao G, Kulatilake PHSW, Liang W, Wang E (2019c) Fracturing behaviour of sandstone specimens with a cavity formed by intersecting excavations under compression: Experimental study and numerical modelling Strain 55:e12316 doi:https://doi.org/10.1111/str.12316

Yang S-Q, Liu X-R, Jing H-W (2013) Experimental investigation on fracture coalescence behavior of red sandstone containing two unparallel fissures under uniaxial compression International Journal of Rock Mechanics and Mining Sciences 63:82-92 doi:https://doi.org/10.1016/j.ijrmms.2013.06.008

Yang X, Kulatilake PHSW, Jing H, Yang S (2015) Numerical simulation of a jointed rock block mechanical behavior adjacent to an underground excavation and comparison with physical model test results Tunnelling and Underground Space Technology 50:129-142 doi:https://doi.org/10.1016/j.tust.2015.07.006

Zhang P, Li N, Li X-b, Nordlund E (2009) Compressive failure model for brittle rocks by shear faulting and its evolution of strength components International Journal of Rock Mechanics and Mining Sciences 46:830-841 doi:https://doi.org/10.1016/j.ijrmms.2009.01.002

Zhuang X, Chun J, Zhu H (2014) A comparative study on unfilled and filled crack propagation for rock-like brittle material Theoretical and Applied Fracture Mechanics 72:110-120 doi:https://doi.org/10.1016/j.tafmec.2014.04.004

Figures

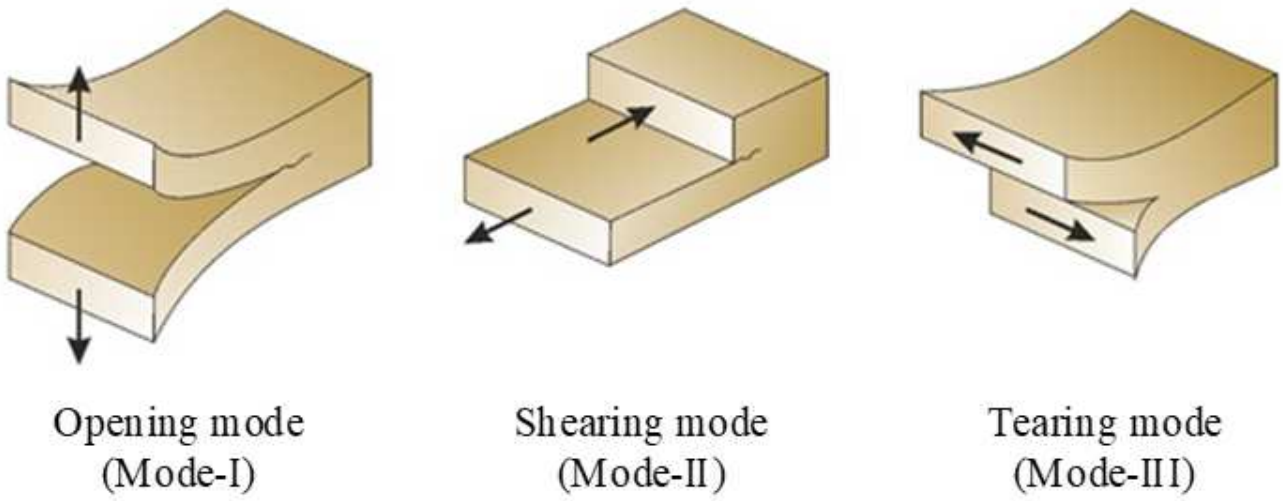

Figure 1

Basic modes of crack extension

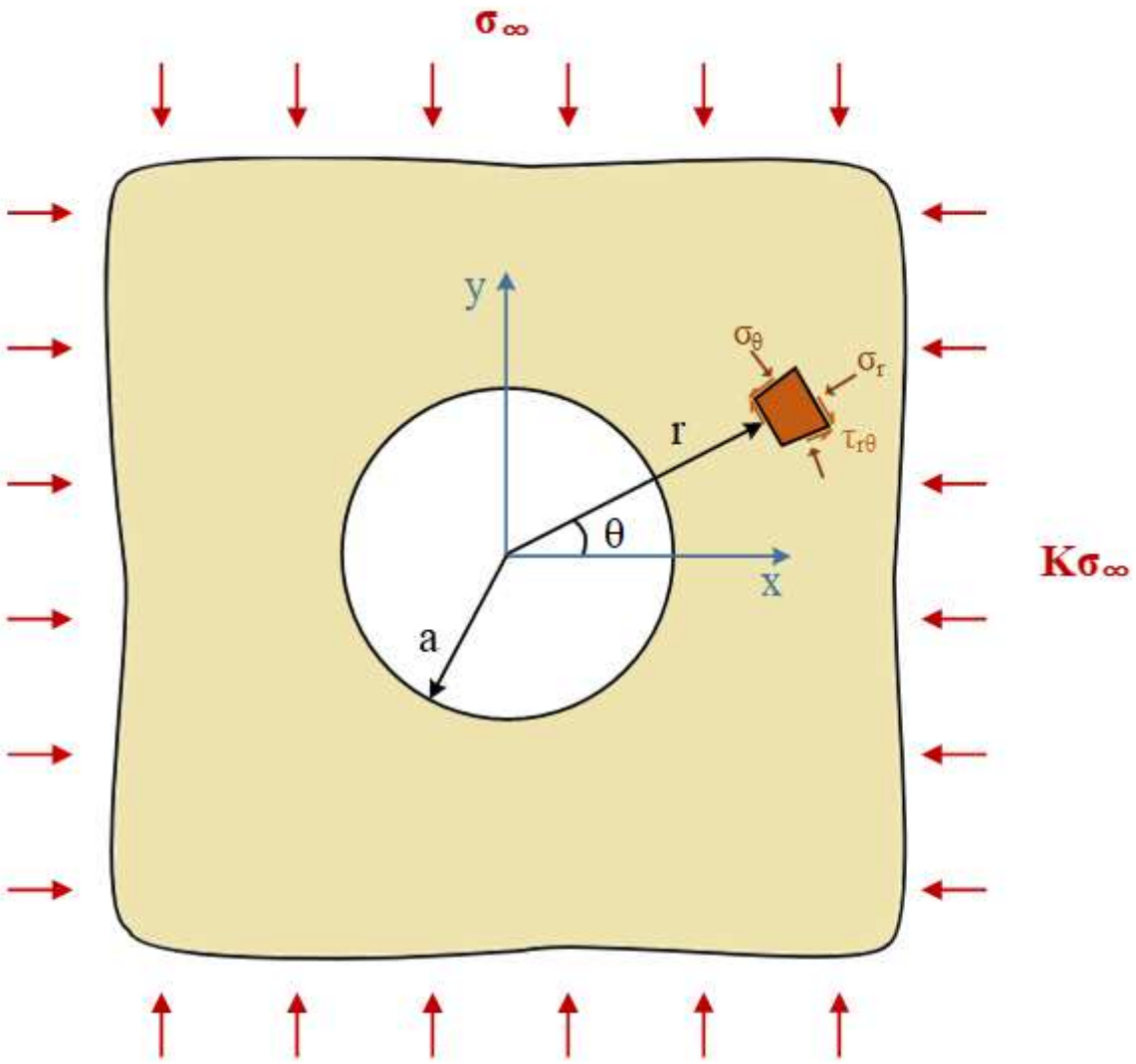

Figure 2

The used coordinate system to express the stress state around a circular hole in a two directional stress field

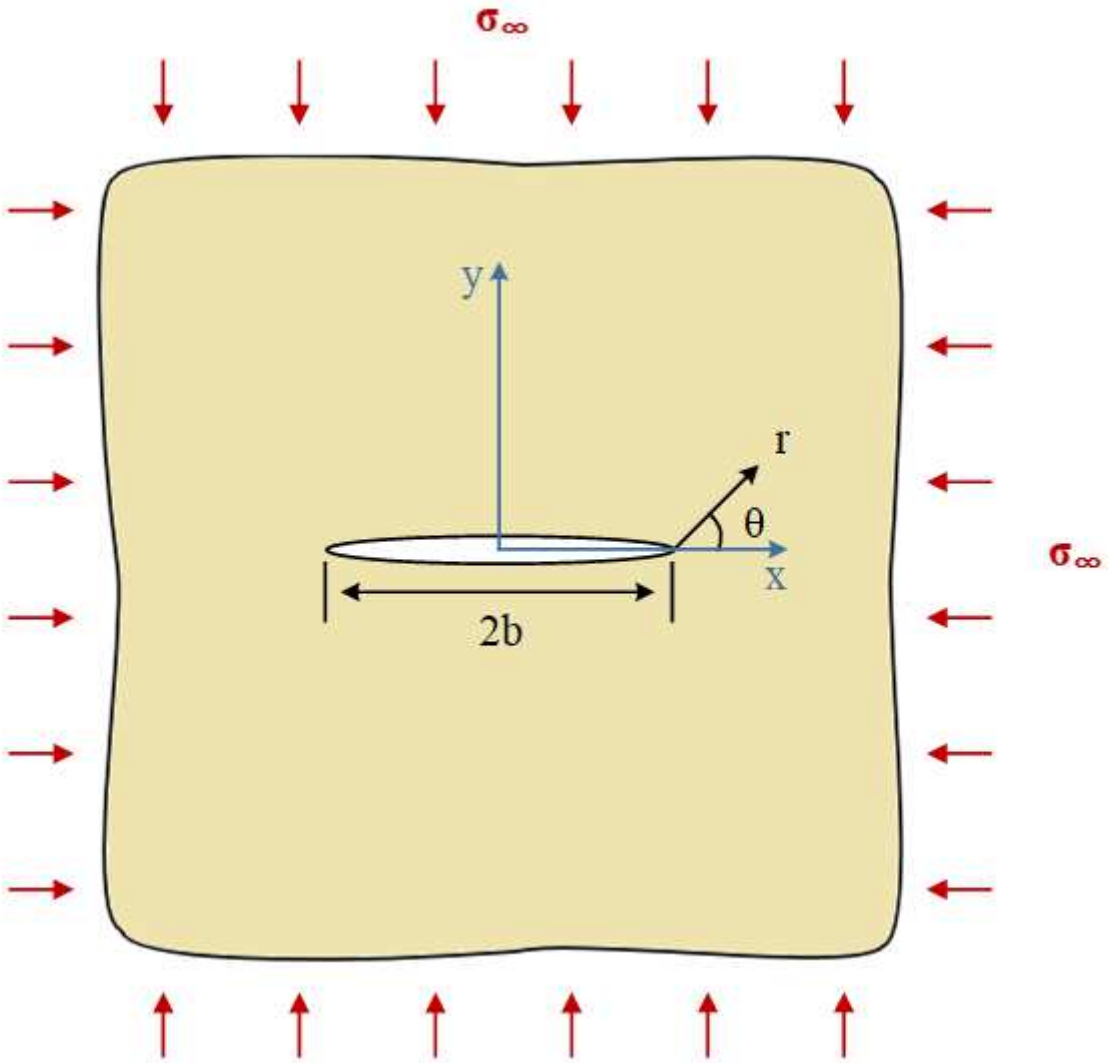

Figure 3

The used coordinate system to express the stress state near a crack tip in a two directional stress field

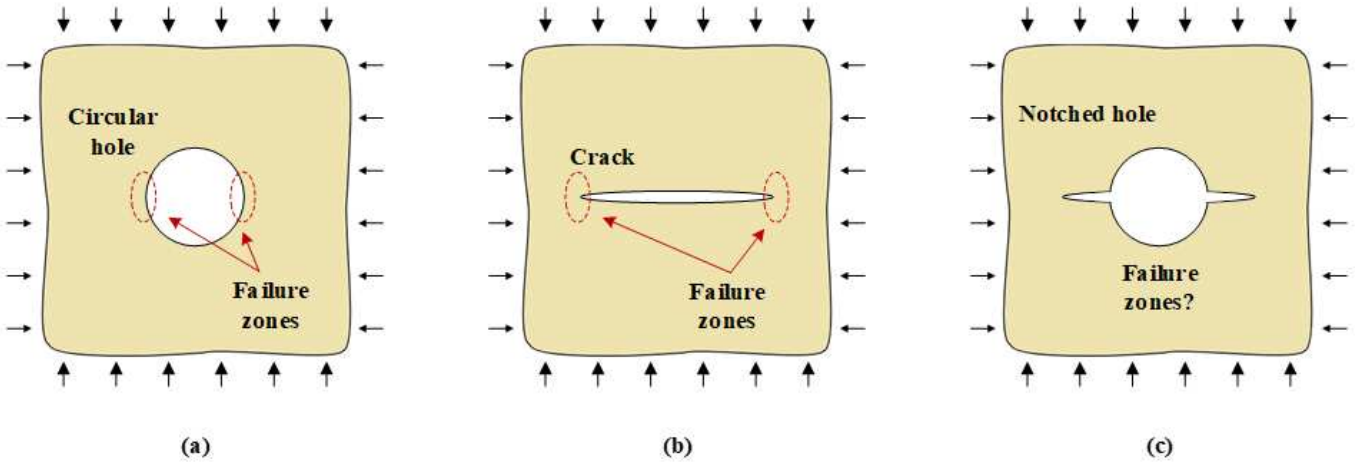

Figure 4

Failure zones in specimens with (a) a circular hole, (b) a crack, and (c) a notched hole under compression

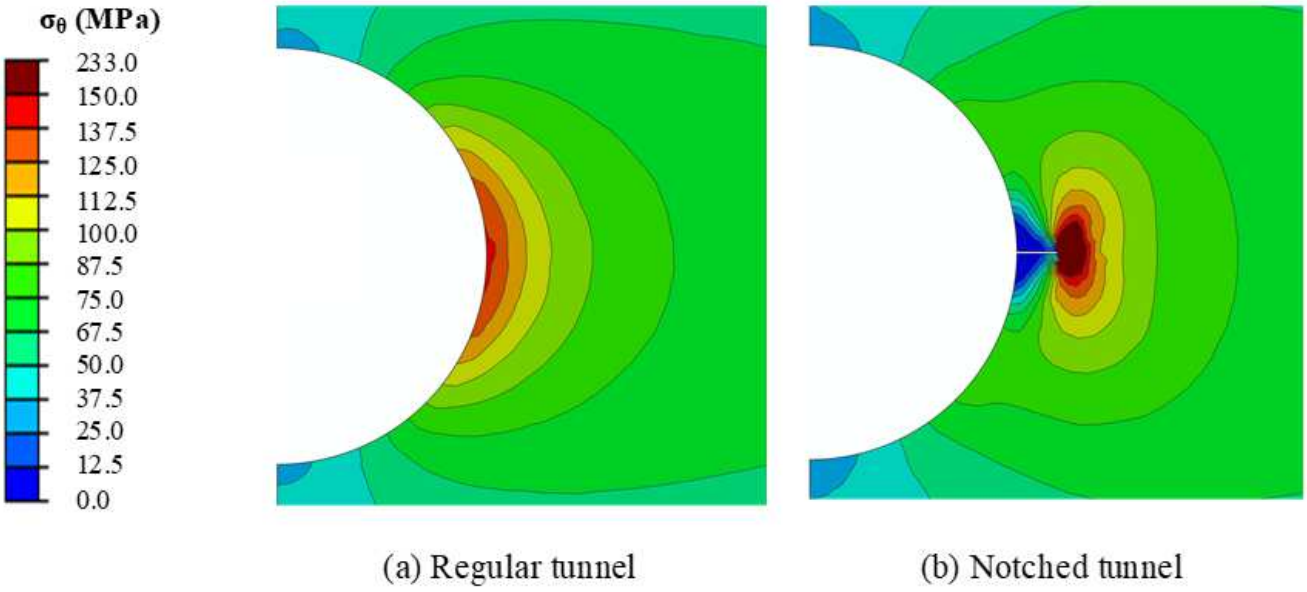

Figure 5

The tangential stress distribution around (a) a regular tunnel and (b) a notched tunnel

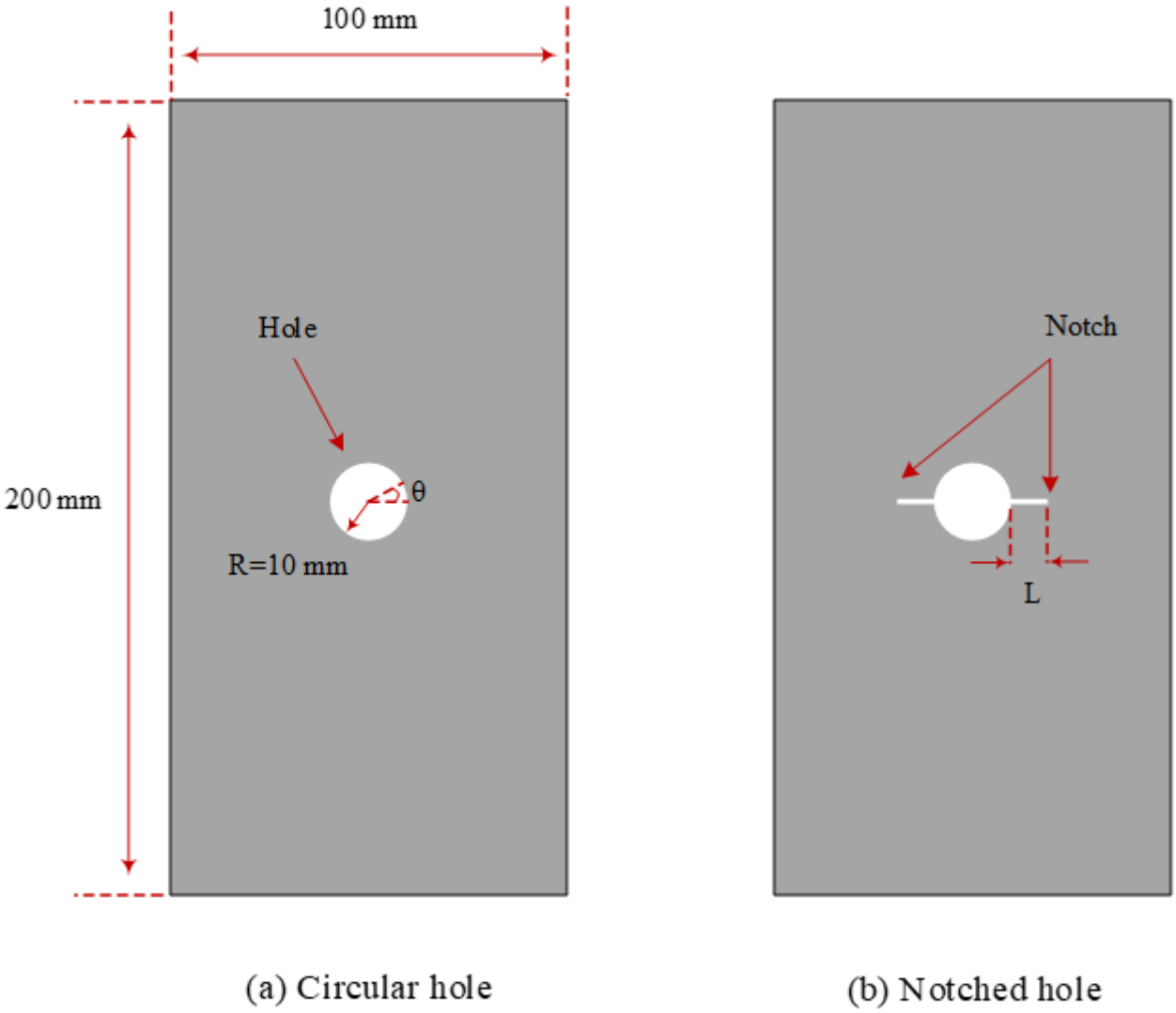

Figure 6

Geometry of the models with (a) a circular hole and (b) a notched hole

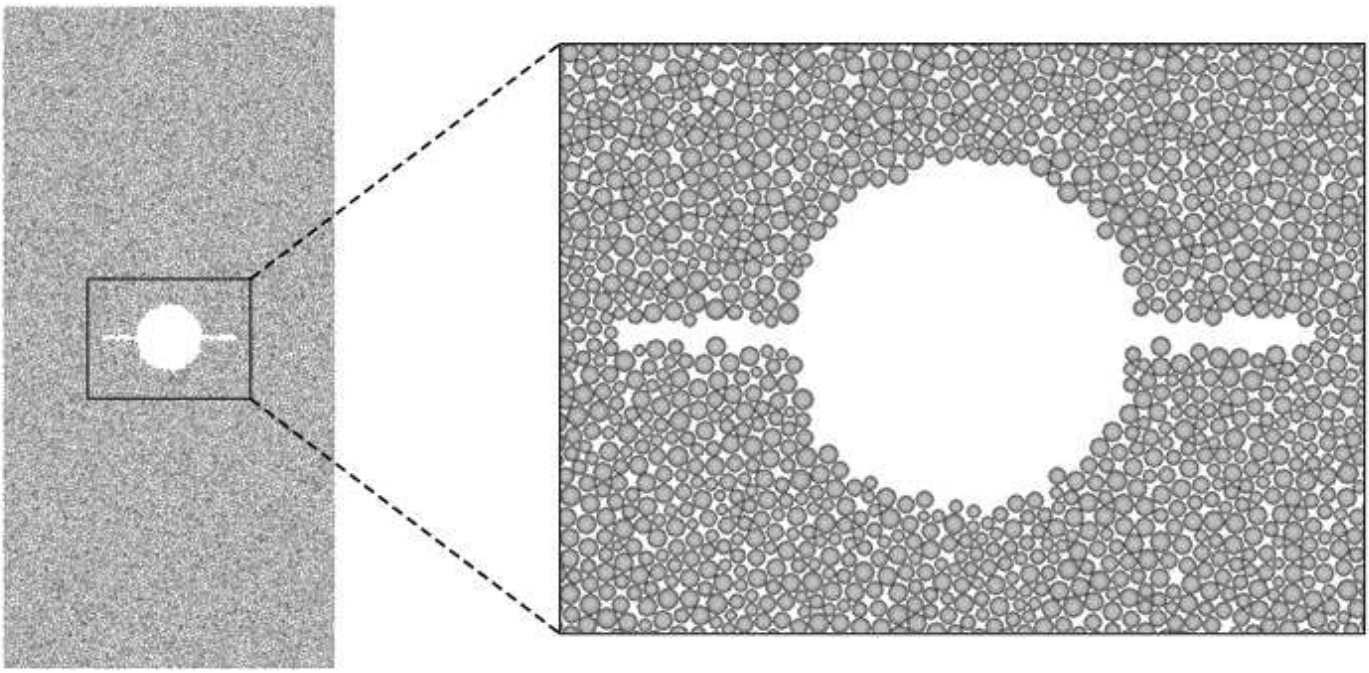

Figure 7

Particle assembly in the notched hole model (L = 10 mm)

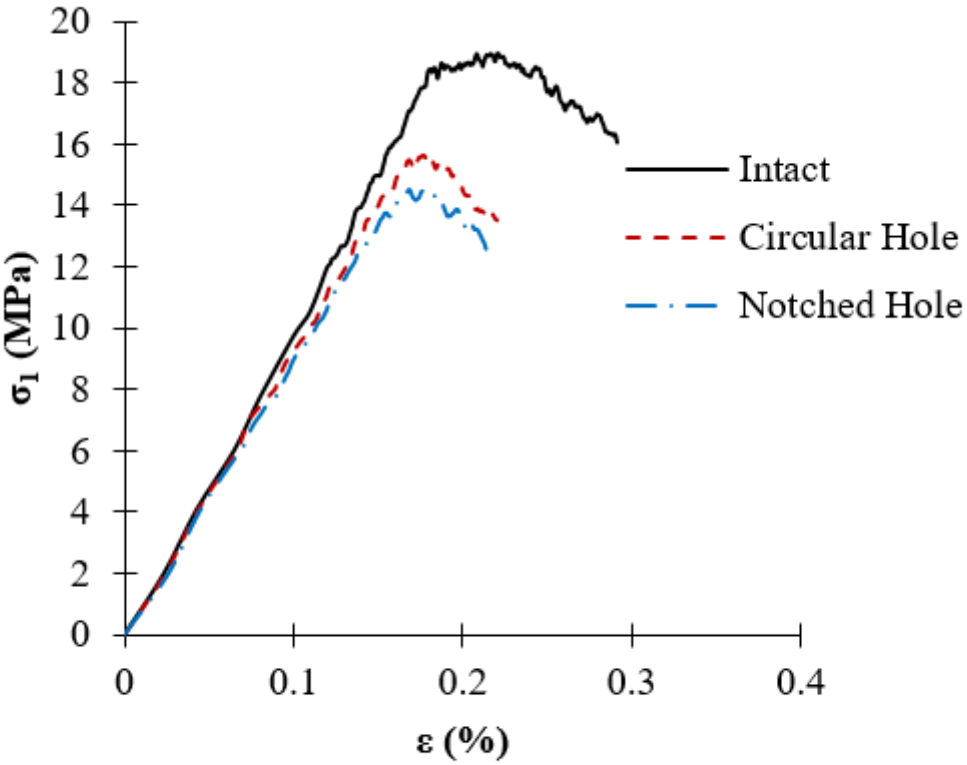

Figure 8

The stress-strain curves obtained from PFC2d models

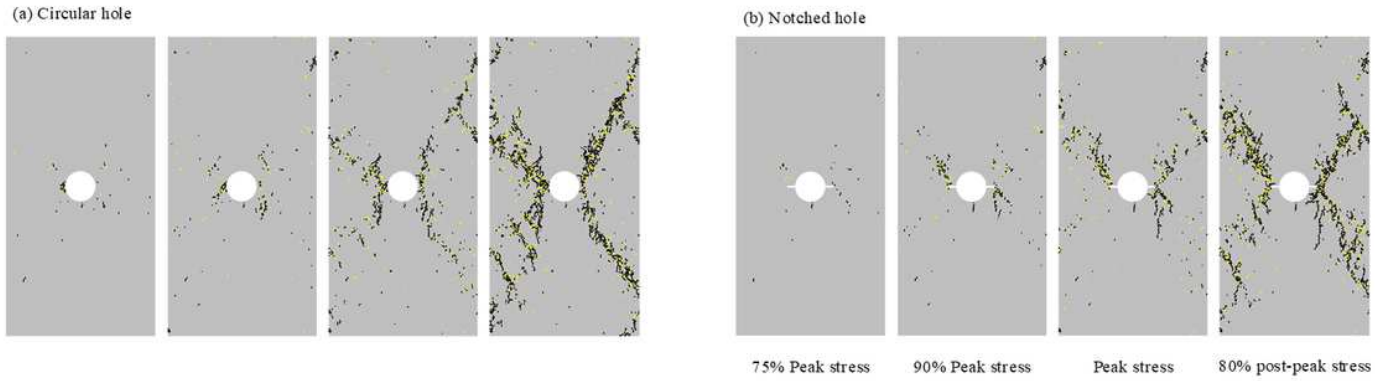

Figure 9

Failure evolution in (a) circular hole, and (b) notched hole (Black and yellow lines represent tensile and shear cracks, respectively)

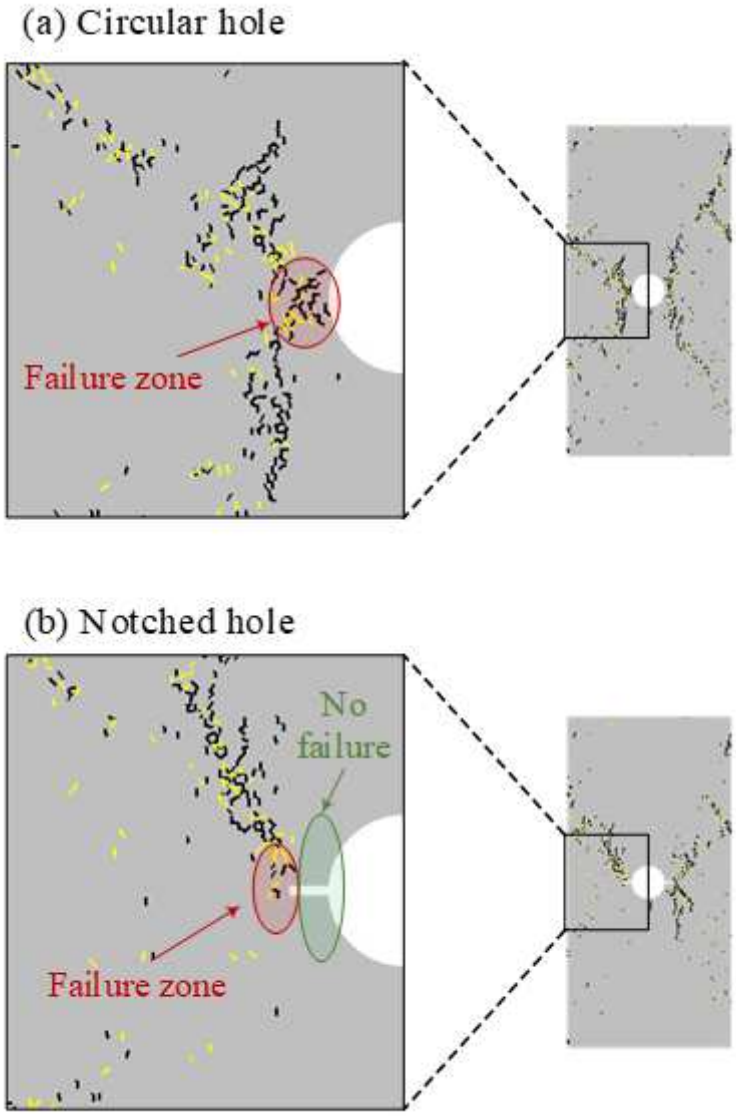

Figure 10

The close views of failure zones around at left side of the hole at peak-stress in the models with (a) a circular hole, and (b) a notched hole with L = 5 mm

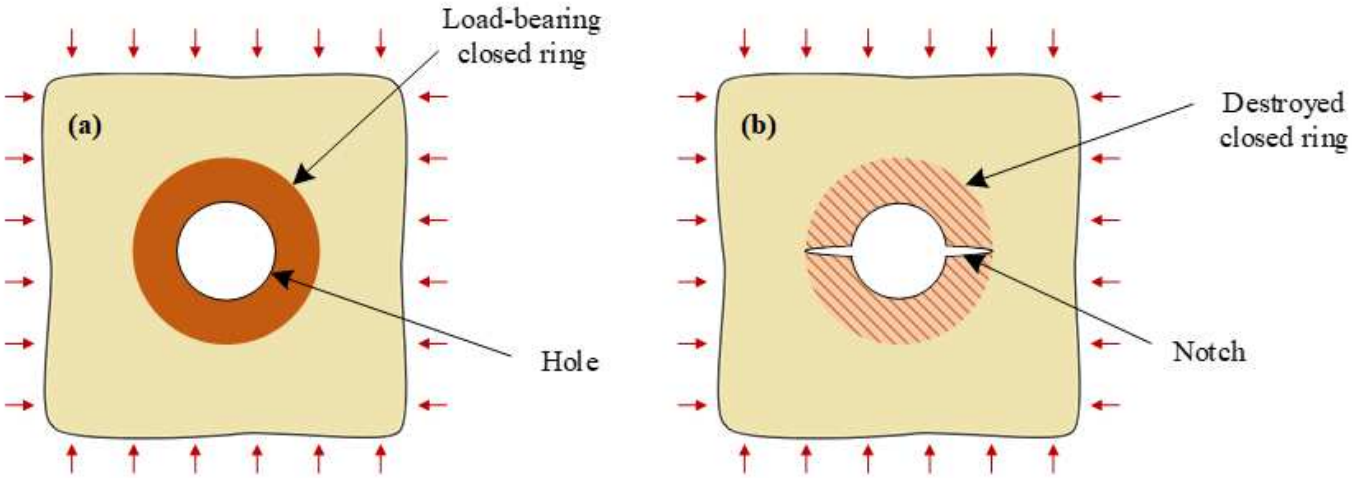

Figure 11

Illustration of the load bearing closed ring around a circular hole

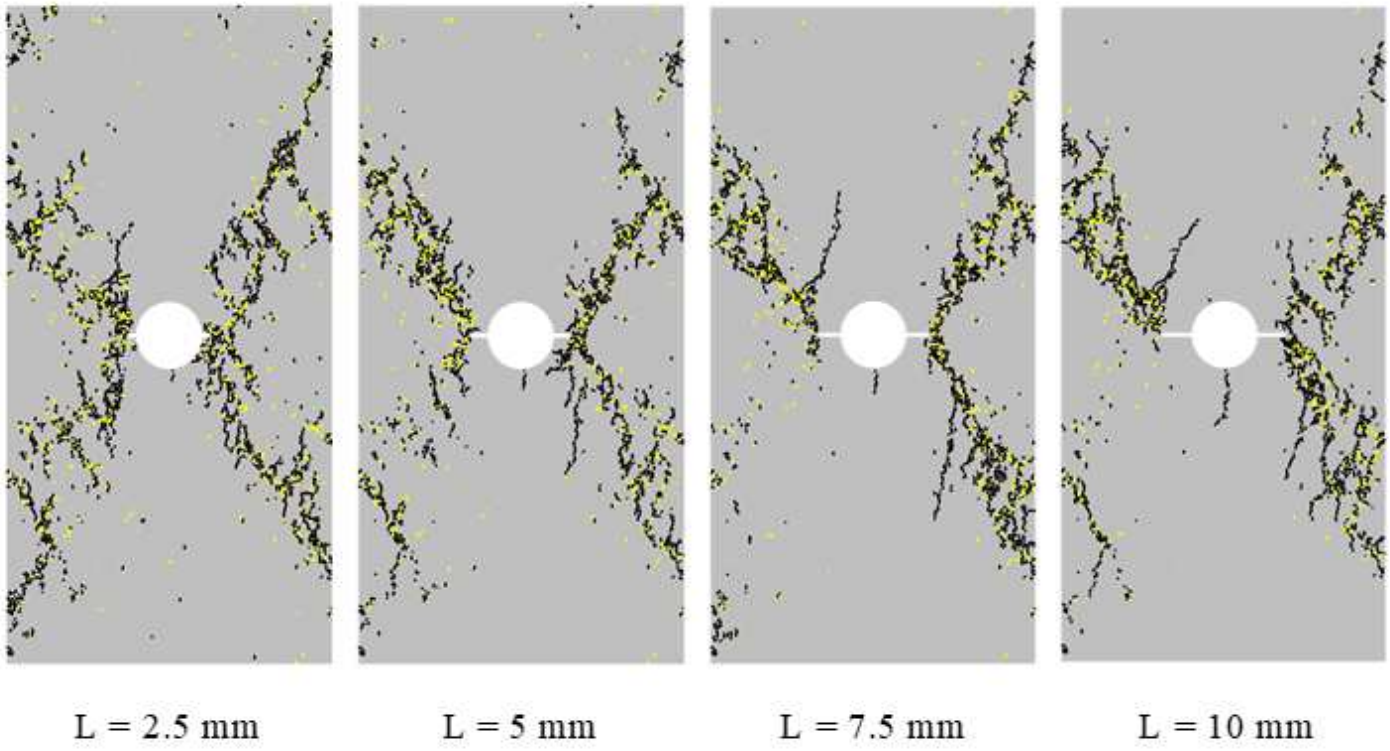

Figure 12

The failure patterns in the models with different notch lengths (80% post-peak stress)

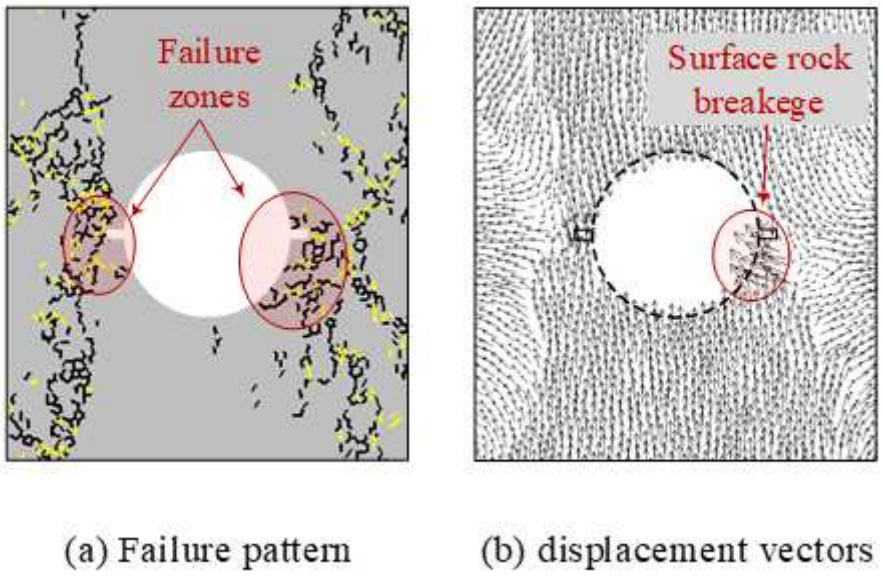

Figure 13

Failure pattern and displacement vector distribution around the notched hole with L = 2.5 mm (L/R ratio of 0.25)

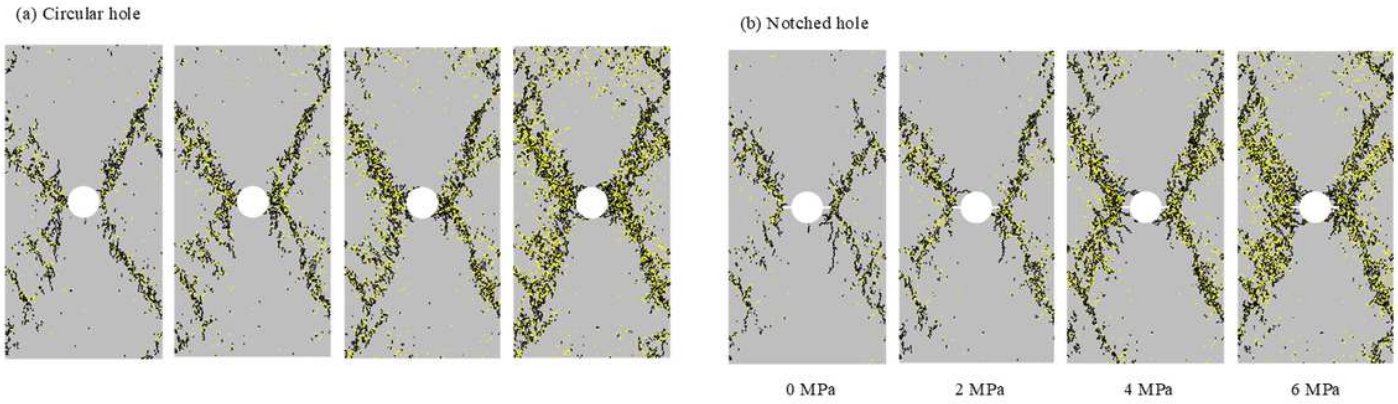

Figure 14

Failure patterns in the (a) circular hole and (b) notched hole models at 80% post-peak stress level for different confining pressures

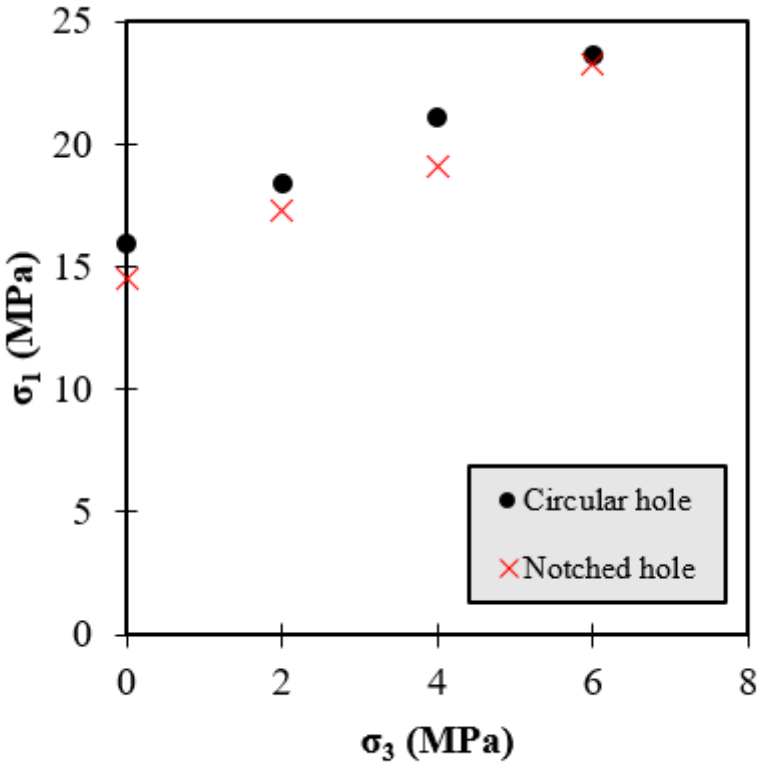

Figure 15

The peak strength at different confining pressures in the two models